Solvation and Polarization of the *N*-Methyl Amine Molecule in Aqueous Solution: A Combined Study of Quantum Mechanics and Integral Equation Theory in Three Dimensions

Qishi Du* and Dongqing Wei

College of Chemistry and Life Sciences and Institute of Bioinformatics and Drug Discovery, Tianjin Normal University, 241 Weijin Road, Hexi District, Tianjin, China 300074

Received: November 26, 2002; In Final Form: September 6, 2003

In this paper, we present a combined approach of quantum mechanics and statistical mechanical integral equation theory in three dimensions to describe the solute−solvent electrostatic interaction and mutual polarization in an infinitely dilute solution of a polar solute molecule in polar solvent. In this combined method, the integral equation theory 3d-RISM-HNC (*J. Phys. Chem. B* **2000**, *104*, 796) provided the average solvent particle densities and solvent charge distribution surrounding a solute molecule. The Schrödinger equation of the solute molecule in solvent background charges was solved with the quantum mechanical SCF Hartree−Fock (HF) method. The electrostatic potentials were calculated using the electronic density of the solute, which can be fitted to the atomic ESP charges. Those charges were, in turn, used in 3d-RISM-HNC calculations, which were solved iteratively. We have seen a significant increase in the solute dipole moment and the solute−solvent electrostatic interaction energy. In the case study of *N*-methyl amine in liquid water, we observed higher hydrogen density of water near O(CO) and higher oxygen density of water near H(NH). It has been shown that the mutual polarization between solute and solvent has significant effect on the thermodynamic properties.

I. Introduction

The solute−solvent interactions and polarization are important aspects of theoretical chemistry. A challenge in the studies of solvation and solvent effects is to incorporate explicitly the polarization effects into the potential surface.[1−7] However, due to the complexity of solute−solvent electrostatic interactions, it has proven difficult to find a simple solution. The problem arises from the difficulty of how to describe the electron structure change of a solute molecule and the change of solvent density distribution in solution alternatively. If one treats the solute−solvent interactions at the ab initio level, it is almost impossible because one has to include a huge number of solvent molecules in the quantum mechanical calculations.

Significant efforts have been made in the last several decades in combining quantum mechanics with classical mechanics, i.e., QM/MM in order to include polarization in a systematic way, such as molecular dynamics (MD)[8−10] and the Monte Carlo (MC) simulations,[10,11] the continuum solvent models,[12,13] and statistical mechanical integral equation theory.[14] A simplified approach was proposed by Chen et al.,[13] a combined method of DFT (density functional theory) and continuum medium Poisson model. The electronic structure of the solute is described by the quantum mechanical density functional theory, and electrostatic features of the environmental effects are modeled through external charge distribution and continuum dielectrics. The Born reaction potential produced by atom-centered point charges and dipoles, fitted to the molecular charge distribution, is computed via finite difference solution to the Poisson−Boltzmann equation. The coupling of the molecular Hamiltonian is achieved through numerical integration, and the entire system is iterated to self-consistency.

A few groups[10] use a semiempirical quantum mechanical−molecular mechanical (QM/MM) simulation method to determine the contribution of the solvent polarization and the total interaction energies between solute and solvents for the amino acid side chains and nucleotide bases in aqueous solution. In an AM1-TIP3 approach, the solute molecule is characterized using valence electrons and nucleus cores with the Hartree−Fock (HF) theory, incorporating explicit solvent effects into the total Hamiltonian, while the solvent is characterized as the three-point charge TIP3 model. A similar combination of the DFT and molecular mechanics/dynamics simulations[8,9] has been applied to study proton transfer in water and enzyme catalysis.

Hirata et al.[14] presented a combined method of the reference interaction site model (RISM) integral equation theory and the ab initio self-consistent (SCF)HF where the hyper-netted chain (HNC) approximation is employed in solving the RISM Ornstein−Zernike equation and determining the solvent distribution around a solute. The electronic structure of the solute molecule is obtained by ab initio SCF calculations. The solvent effective potential modifying the electronic structure of the solute molecules was incorporated by adding a solvent term to the Fock operator.

To improve the accuracy of the RISM-HNC theory, recently, Du, Beglov, and Roux[15] introduced the empirical water hydrogen and oxygen bridge functions. The calculated solvation free energies are in good accord with the experimental data. Without the bridge functions, the results are quite poor. In this paper, we present results of the combined RISM integral equation theory with the SCF MO approach using the optimized bridge functions. In our combined QM-RISM approach, we adapted a

* Corresponding author. Tel: 086-22-2354-0310. Fax: 086-22-2351-4100. E-mail: duqishi@yahoo.com.

10.1021/jp022493v CCC: $25.00
Published on Web 11/13/2003

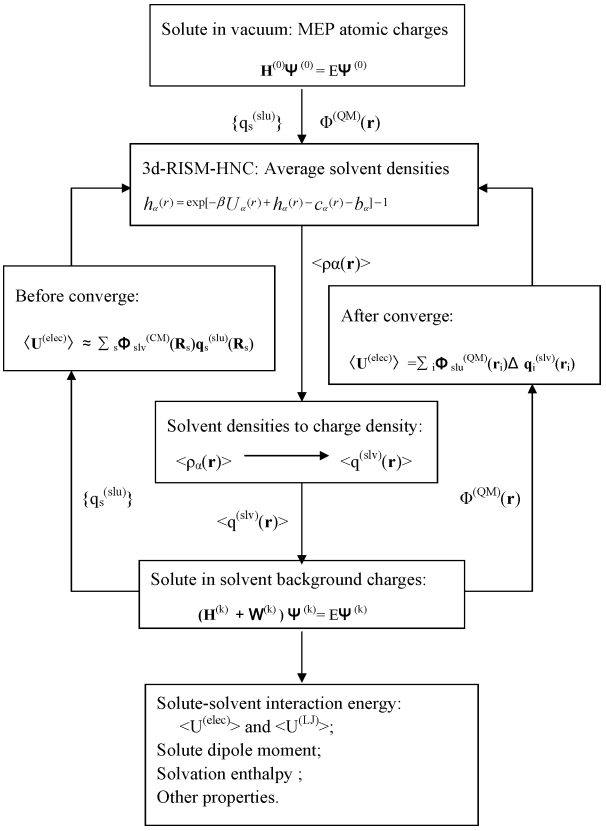

Figure 1. The flow chart of the combined quantum mechanical and statistical mechanical integral equation theory in three dimensions, QM/3d-RISM-HNC.

simpler approach comparing with Hirata et al.[14] The solvent average particle densities, $\langle\rho_\alpha(\mathbf{r})\rangle$, for example, in liquid water, the oxygen particle density $\langle\rho_O(\mathbf{r})\rangle$, and the hydrogen particle density, $\langle\rho_H(\mathbf{r})\rangle$, are calculated using the statistical mechanical integral equation theory, 3d-RISM-HNC. Then, the solvent charge density distributions are easily derived from solvent particle densities. The solute−solvent electrostatic interaction energy is updated from the quantum mechanical ab initio calculations.[16] The Schrödinger equation of the solute molecule is solved in the solvent background charges. The ESP (electrostatic potential) equivalent atomic charges $q_s^{(slu)}$ are used in 3d-RISM-HNC calculations in the next iterative cycle, and new background charges for the quantum mechanical calculation of the solute molecule can be achieved with the updated solvent particle densities. We then applied the theoretical methods to study the solvation of a *N*-methyl amine (NMA) molecule in liquid water. Some very interesting results have been obtained.

For the completeness of this article, we give detailed accounts of the theoretical methods in the next section. The computational details, results, and discussion are given the following sections.

II. Theoretical Developments

The basic idea of our method is illustrated in the Figure 1. As a starting point of iteration, we consider a solute molecule isolated in a vacuum. The electronic structure of the solute molecule is described by the Schrödinger equation

$$\boldsymbol{H}^{(0)}\Psi^{(0)} = E\Psi^{(0)} \tag{1}$$

where $\boldsymbol{H}^{(0)}$ is the Hamiltonian of the solute molecule in a vacuum and superscript (0) refers to the zero-order approximation for the solute molecule in solution. When the solute molecule is placed into liquid, due to the electrostatic potential field of the solute molecule, the density distribution of solvent molecules surrounding the solute molecule is described by the average solvent particle densities, $\langle\rho_\alpha(\mathbf{r})\rangle$, as given by the 3d-RISM-HNC integral equation

$$h_\alpha(\mathbf{r}) = e^{[-\beta U_\alpha(\mathbf{r}) + h_\alpha(\mathbf{r}) - c_\alpha(\mathbf{r}) - b_\alpha(\mathbf{r})]} - 1 \tag{2}$$

where $b_\alpha(\mathbf{r})$ is the bridge function[15] and $h_\alpha(\mathbf{r})$ is the solute−solvent site correlation function

$$h_\alpha(\mathbf{r}) = \langle\rho_\alpha(\mathbf{r})\rangle/\bar{\rho} - 1 \tag{3}$$

In eq 2, $c_\alpha(\mathbf{r})$ is the solute−solvent direct correlation function defined by

$$\bar{\rho}h_\alpha(\mathbf{r}) = \sum_\gamma c_\gamma * \chi_{\gamma\alpha}(\mathbf{r}) \tag{4}$$

where $\chi_{\gamma\alpha}(\mathbf{r})$ is the solvent susceptibility response function of pure liquid and the asterisk symbol represents a spatial convolution in three-dimensional space. By convention, the Greek letter α is for the solvent interaction sites and the letter *s* is for the solute interaction sites. In 3d-RISM-HNC, the interaction sites are component atoms of the solute and solvent molecules. Therefore, α and *s* are atomic indices of the solute and solvent molecules, respectively.

In eq 2, $\boldsymbol{U}_\alpha(\mathbf{r})$ is the solute−solvent interaction potential energy on solvent site α, which consists of the van der Waals and electrostatic part, respectively

$$\boldsymbol{U}_\alpha(\mathbf{r}) = \sum_s U_{\alpha,s}^{(LJ)}(|r - r_s|) + \sum_s U_{\alpha,s}^{(elec)}(|r - r_s|) \tag{5}$$

All solvent effects and thermodynamic properties can be calculated directly from the average densities $\langle\rho_\alpha(\mathbf{r})\rangle$. The average van der Waals interaction energy of solute and solvent, $\langle\boldsymbol{U}^{(LJ)}\rangle$, in our previous work, is evaluated with the distance-dependent Lennard-Jones 6-12 potential. The average electrostatic interaction energy of the solute and solvent molecules, $\langle\boldsymbol{U}^{(elec)}\rangle$, is computed based on the classical Coulomb law

$$\langle\boldsymbol{U}^{(elec)}\rangle = \int dr \sum_\alpha \sum_s \boldsymbol{U}_{\alpha,s}^{(elec)}(\mathbf{r})\langle\rho_\alpha(\mathbf{r})\rangle \tag{6}$$

In eq 6, the summation index α is over all solvent interaction sites and index *s* is over all solute interaction sites. In this paper, we calculate the electrostatic part of solute−solvent interaction energy using quantum mechanics. A solute molecule in solution can be described using the Schrödinger equation

$$(\boldsymbol{H}^{(k)} + \boldsymbol{W}^{(k)})\Psi = E^{(k)}\Psi \tag{7}$$

In eq 7, index *k* is the iteration number, $\boldsymbol{H}^{(k)}$ is the Hamiltonian of the solute molecule, and $\boldsymbol{W}^{(k)}$ is due to the solvent perturbation. Here, we only consider the solvent electrostatic perturbation, therefore, $\boldsymbol{W}^{(k)}$ is an electrostatic interaction operator. By combination of quantum mechanics with 3d-RISM-HNC, we get the average solute−solvent electrostatic interaction energy

$$\langle\boldsymbol{U}^{(elec)}\rangle = \int dr\, \Phi_{slu}^{(QM)}(\mathbf{r})\langle q_{slv}(\mathbf{r})\rangle \tag{8}$$

where the average solvent charge distribution $\langle q_{slv}(\mathbf{r})\rangle$ is

evaluated using the particle average densities $\langle\rho_\alpha(\mathbf{r})\rangle$ and particle charges q_α on solvent site α

$$\langle q_{\mathrm{slv}}(\mathbf{r})\rangle = \sum_\alpha q_\alpha \langle\rho_\alpha(\mathbf{r})\rangle \tag{9}$$

In eq 8, $\Phi_{\mathrm{slu}}^{(\mathrm{QM})}(\mathbf{r})$ is the quantum mechanical electrostatic potential of the solute molecule at position $\mathbf{r}$

$$\Phi_{\mathrm{slu}}^{(\mathrm{QM})}(\mathbf{r}) = \sum_s \frac{Z_s}{||r - R_s||} - \int_\infty \frac{\rho^{(\mathrm{e})}(\mathbf{r}')}{||r - r'||}\,\mathrm{d}r' \tag{10}$$

The electronic density of solute molecule in eq 10, $\rho^{(\mathrm{e})}(\mathbf{r}')$, is obtained from the wave function of the solute molecule

$$\rho^{(\mathrm{e})}(\mathbf{r}) = \langle\Psi|\hat{\rho}(\mathbf{r})|\Psi\rangle = \sum_{i=1}^{\mathrm{occ}} n_i \sum_\mu \sum_\nu c_{\mu i} c_{\nu i} \varphi_\mu(\mathbf{r})\varphi_\nu(\mathbf{r}) \tag{11}$$

where n_i is the occupation number.

In 3d-RISM-HNC, we use a cubic grid, $N = 128^3$, in the solute and solvent space. The solute−solvent average electrostatic interaction energy can be evaluated numerically by the summation of products of the solvent charge elements and quantum mechanical solute electrostatic potentials $\Phi_{\mathrm{slu}}^{(\mathrm{QM})}(\mathbf{r}_i)$ over all points in the cubic grid surrounding solute space

$$\langle \boldsymbol{U}^{(\mathrm{elec})}\rangle = \sum_{i=1}^{N} \Phi_{\mathrm{slu}}^{(\mathrm{QM})}(\mathbf{r}_i)\Delta q_i^{(\mathrm{slv})}(\mathbf{r}_i) \tag{12}$$

where $\Delta q_i^{(\mathrm{slv})}(\mathbf{r}_i)$ is the solvent charge element

$$\Delta q_i^{(\mathrm{slv})} = \sum_\alpha q_\alpha \langle\rho_\alpha(\mathbf{r}_i)\rangle \Delta V_i \tag{13}$$

It is the product of solvent particle charges and grid volume elements, and summation is over the solvent interaction sites. Actually, in each volume element we keep two charge elements, one is a positive charge, another is a negative charge. They are located on their charge mass centers in the cubic grid elements.

The quantum mechanical calculations of electrostatic potentials at 128^3 points represent a huge workload. Convergence of the 3d-RISM-HNC/QM iterations may need hundreds of iteration cycles. In the present study, we use an alternative and simpler method to calculate average solute−solvent electrostatic interaction energy $\langle \boldsymbol{U}^{(\mathrm{elec})}\rangle$. The ESP (electrostatic potential) equivalent atomic charges $q_s^{(\mathrm{slu})}$ of the solute molecule are evaluated at the RHF/6-31G(d) level and are used in 3d-RISM-HNC calculations. The average solute−solvent electrostatic interaction energy can be calculated in another way

$$\langle \boldsymbol{U}^{(\mathrm{elec})}\rangle \approx \sum_{s=1}^{M} \Phi_{\mathrm{slv}}^{(\mathrm{CM})}(\mathbf{R}_s) q_s^{(\mathrm{slu})}(\mathbf{R}_s) \tag{14}$$

where $\Phi_{\mathrm{slv}}^{(\mathrm{CM})}(\mathbf{R}_s)$ is the classical mechanical electrostatic potential produced by all solvent charges at nuclear position $\mathbf{R}_s$ of atom s in the solute molecule

$$\Phi_{\mathrm{slv}}^{(\mathrm{CM})}(\mathbf{R}_s) = \sum_{s=1}^{N} \frac{\Delta q_i^{(\mathrm{slv})}}{||R_s - r_i||} \tag{15}$$

Unlike the Mulliken atomic charges, in eq 14, the ESP equivalent atomic charges $q_s^{(\mathrm{slu})}$ reproduce the electrostatic potentials in molecular space close to the quantum mechanical electrostatic potentials mostly. Therefore, we have chosen ESP instead of the Mulliken charges. The difference between classical and quantum results should not significant. However, the calculation workload based on classical eqs 14 and 15 is much smaller than that from the quantum mechanical eqs 10 and 12.

This way, the HF−SCF and 3d-RISM-HNC calculations can be carried out in an affordable time scale for real organic molecules in liquid water. As it is shown in Figure 1, in each cycle of iteration, the QM calculations of the solute molecule provide the ESP atomic charges of the solute molecule, which are used in the next cycle of the 3d-RSIM-HNC calculations. Then the 3d-RISM-HNC calculations give the average solvent particle densities, from which we get the average solvent charge distribution and it provides a background charge in the next cycle of the QM calculation. After the iterations converge, we will recalculate the solute−solvent average electrostatic interaction energy $\langle \boldsymbol{U}^{(\mathrm{elec})}\rangle$ using eqs 10 and 12 and then compare it with the results obtained from classical mechanical eqs 14 and 15.

III. Computational Detail

In the 3d-RISM-HNC calculations, we use a $N = 128^3$ cubic grid with spacing of 0.225 Å, corresponding to an elementary cell of 28.8 Å. The water TIP3 model[19] is used. The partial charges of oxygen and hydrogen are $q_{\mathrm{O}} = -0.834\ e$ and $q_{\mathrm{H}} = 0.417\ e$, respectively. The LJ parameters of oxygen are $\sigma_{\mathrm{OO}} = 3.1507$ Å and $\epsilon_{\mathrm{OO}} = 0.152073$ kcal/mol; the length of the OH bond is $l_{\mathrm{OH}} = 0.9572$ Å. No LJ interaction site was assigned to the hydrogen.[19] As in the previous works,[17,18] the solvent susceptibility of bulk water was calculated on the basis of the standard RISM-HNC theory and stored in k space.[20] The average density of pure water is 0.334 Å^{-3}, and temperature is 298.15 K. The LJ parameters for NMA are taken from the CHARMM22 force field.[18] We used the Gaussian 94 program package[16] at RHF/6-31G(d) level to perform the QM calculations.

Each cycle of the QM/3d-RSIM-HNC iteration contains two separated iterations. One is the HF−SCF iteration, and another is the 3d-RISM-HNC iteration. The converge criteria of HF−SCF is that of Gaussian 94; the difference of trace of density matrix between two cycles is smaller than $\epsilon < 10^{-8}$. The converge criteria of the 3d-RISM-HNC iteration is the differences between new and old direct correlation functions that are set to be smaller than 2.00×10^{-4} over all grid points, i.e., $|\mathrm{C}_\alpha^{(\mathrm{new})} - \mathrm{C}_\alpha^{(\mathrm{old})}| < 2.00 \times 10^{-4}$. The converge criteria of the combined QM/3d-RISM-HNC iteration is that the average solute−solvent interaction energy is smaller than 0.1 kcal/mol, i.e., $|\mathrm{U}^{(\mathrm{LJ+elec})}(\mathrm{new}) - \mathrm{U}^{(\mathrm{LJ+elec})}(\mathrm{old})| < 0.1$ kcal/mol.

The particle average density distributions of oxygen and hydrogen, $\langle\rho_{\mathrm{O}}(\mathbf{r})\rangle$ and $\langle\rho_{\mathrm{H}}(\mathbf{r})\rangle$, on the 128^3 cubic grid are converted into the solvent charge density distributions, $\Delta q^{(\mathrm{slv})}(\mathbf{r}_i)$. In the quantum mechanical calculations of the solute molecule in the solvent background charges, the total number of solvent charges is reduced from 128^3 to 32^3, to lower the calculation workload. In each cell of the 32^3 grid, we keep two charges, $\Delta q_+^{(\mathrm{slv})}(\mathbf{r}_i)$ and $\Delta q_-^{(\mathrm{slv})}(\mathbf{r}_i)$. One is the average weighted positive charges, and another is the average weighted negative charges. The charge centers are their charge mass centers. The

formulas we used are as follows

$$\Delta q_i^+ = \sum_{j=1}^{16} q_\alpha^+ \langle \rho_\alpha(\mathbf{r}_j) \rangle \Delta V \tag{16}$$

$$x_i^+ = \frac{\sum_{j=1}^{16} x_j \sum_\alpha q_\alpha^+ \langle \rho_\alpha(\mathbf{r}_j) \rangle \Delta V}{\Delta q_i^+} \tag{17}$$

$$y_i^+ = \frac{\sum_{j=1}^{16} y_j \sum_\alpha q_\alpha^+ \langle \rho_\alpha(\mathbf{r}_j) \rangle \Delta V}{\Delta q_i^+} \tag{18}$$

$$z_i^+ = \frac{\sum_{j=1}^{16} z_j \sum_\alpha q_\alpha^+ \langle \rho_\alpha(\mathbf{r}_j) \rangle \Delta V}{\Delta q_i^+} \tag{19}$$

Similar formulation is applicable to the negative charges, $\Delta q_-^{(\mathrm{slv})}(\mathbf{r}_i)$.

In the present study, the quantum mechanical calculations are at the RHF/6-31G(d) level in the presence of the solvent background charge distribution.[16,21] The total solvent point charges are as many as $2 \times 32^3 = 65536$. The ESP atomic charges are obtained by fitting the atomic charges to the QM electrostatic potential at the solute van der Waals molecular surface,[15] and 642 points are used for ESP charge fitting.

In this work, we use the same 3d-RISM-HNC program package as the previous works of Roux's group,[15,18] in which hydrogen and oxygen bridge functions are used in order to improve both electrostatic and van der Waals contribution of solvation free energy. We set a scale factor of hydrogen bridge function $a_H = 0.862$ and the scale factor of oxygen bridge function $a_O = 0.397$, which are optimized in the previous works.[15] Kovalenko and Hirata[22] did the similar thing in their recent work. They added a repulsive bridge correction (RBC) in RISM-HNC approximation for a better description of the hydrophobic solute. Our hydrogen and oxygen bridge functions improve both solute−solvent van der Waals and electrostatic interaction significantly.

IV. Results and Discussion

The changes in water oxygen and hydrogen average densities during iterations reflect the structural change of water from the influence of solute molecule on the solvent molecules. Figure 2 is the three-dimensional distributions of the water oxygen density and hydrogen density surrounding t-NMA. We see higher hydrogen density in the front of O in the C═O group and higher oxygen density in the front of H in the NH group. Figure 3 is the radial distribution of water oxygen and hydrogen average densities ($\langle \rho_O(\mathbf{r}) \rangle$ and $\langle \rho_H(\mathbf{r}) \rangle$) on several atoms of solute molecule t-NMA in liquid water. Results of three iteration cycles (cycles 0, 1, and 5) are shown in Figure 3. We find that the hydrogen density of water around the polar atom O(CO) has the largest increase, and the water oxygen average density around another polar atom H(NH) has the second largest increase. Atoms O(CO) and H(NH) are a hydrogen bond acceptor and donor, respectively, and apparently on these two positions, hydrogen bonds are formed. Density increases of water hydrogen and oxygen on these two positions during the QM/3d-RISM-HNC iteration are the result of mutual polarization between water molecules and t-NMA. Clearly the combined QM/3d-RISM-HNC is sensitive to the hydrogen bonds and solute−solvent mutual polarization. On the nonpolar atoms, particularly on the lipophilic part, say, of methyl group CH_3, we do not see much change in the water hydrogen and oxygen densities.

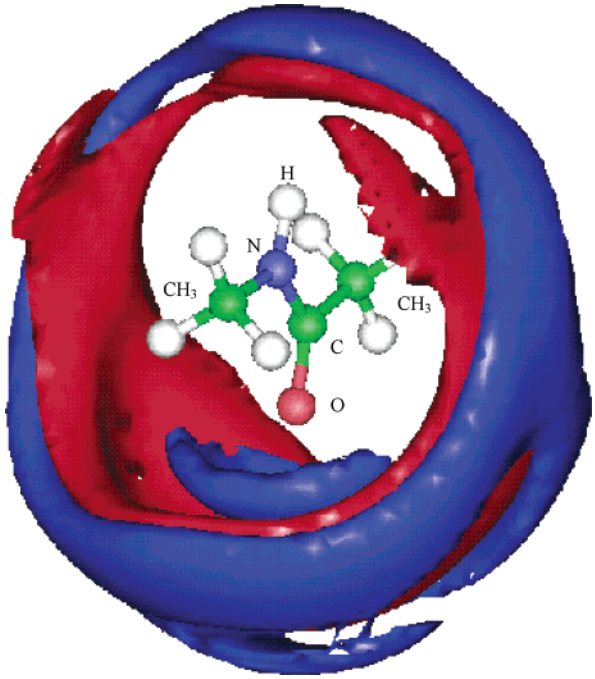

Figure 2. The three-dimensional density distributions of water oxygen and water hydrogen surrounding t-NMA. The blue (dark) represents the hydrogen density of water, and the red (gray) represents the hydrogen density of water. There is higher water hydrogen density in the front of O in the C═O group and higher water oxygen density in the front of H in the NH group.

Figure 4 shows the increase of the dipole moments of t-NMA and c-NMA with the iterations. This is the result of polarization from the charges of the solvent molecules. The dipole moments in cycle 0 are the dipole moments in a vacuum. The dipole moments of t-NMA and c-NMA increase 9% from iteration cycle 1 to cycle 5 (QM/3d-/RISM-HNC iteration converged). The converged value represents the dipole moments of NMA in the liquid phase.

During the iterations, we observe an increase in atomic ESP charges of some atoms in the solute molecule. Figure 5 shows the atomic ESP charges of t-NMA changing as the function of iterations. The largest increases of atomic charges are on C and O in the carbonyl group CO. The positive charge of H in the NH group has a notable increase too. The electrostatic potentials on solute atomic centers produced by solvent charges are shown in Figure 6, where the electrostatic potential on carbonyl oxygen O(CO) has the largest increase. The decrease of the electrostatic potential on H(NH) is the second largest. The positive charged carbon in carbonyl group C(CO) has an unusual positive electrostatic potential. This phenomenon might be explained considering high particle density of water hydrogen surrounding oxygen in the carbonyl group O(CO). The positively charged water hydrogen gives a positive electrostatic potential on positive charged C(CO).

Figure 7 shows the average solute−solvent interaction energies, including the van der Waals and electrostatic contribution. The nonpolar part, $\langle U^{(\mathrm{LJ})} \rangle$, almost keeps constant (getting little bit weaker) during the iterations. On the other hand, the

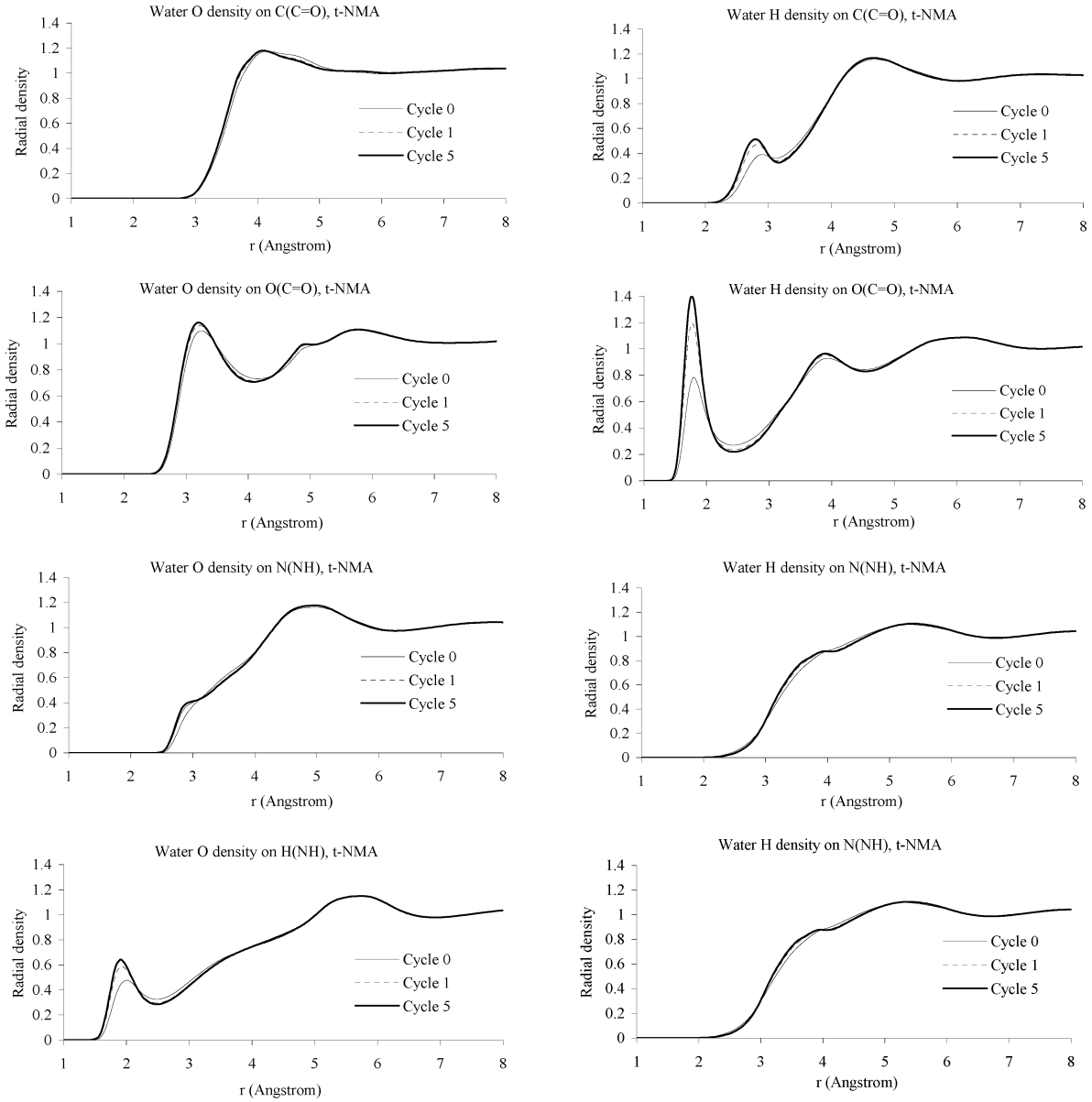

Figure 3. The water oxygen average density $\langle \rho_O(\mathbf{r}) \rangle$ and water hydrogen average density $\langle \rho_H(\mathbf{r}) \rangle$ around C(CO), O(CO), N(NH), and H(NH) of t-NMA. Iteration cycles 0, 1, and 5 of QM/3d-RISM-HNC are shown in the figure.

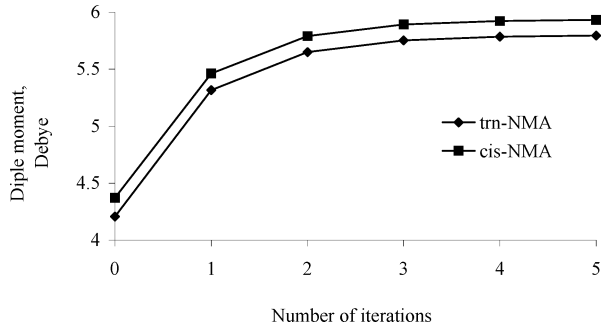

Figure 4. The dipole moments of t-NMA and c-NMA as functions of QM/3d-RISM-HNC iterations. Iteration cycle 0 refers to molecules in a vacuum. Other calculations are in liquid water.

electrostatic part, $\langle \boldsymbol{U}^{(\mathrm{elec})} \rangle$, is getting stronger notably. This is consistent with the increase of the solute dipole moment and ESP charges.

The total energies (including solvent contribution) of t-NMA and c-NMA calculated with the Gaussian 94 at the RHF/6-31G-(d) level are shown in Figure 8a. In iteration cycle 0, t-NMA and c-NMA molecules are actually in a vacuum. From Figure 8a, we can see that the total energies are getting lower during iterations due to the mutual polarization between solute and solvent molecules. The difference of the total energies between t-NMA and c-NMA in water is larger than their difference in a vacuum. The total average solute−solvent interaction energies of t-NMA and c-NMA, $\langle \boldsymbol{U}_{\mathrm{slu-slv}} \rangle$, which is the sum of the electrostatic interaction part and the van der Waals part, are shown in Figure 8b. The total solute energy $\boldsymbol{E}_{\mathrm{slu}}^{(\mathrm{total})}$ is the sum of the solute energy $\boldsymbol{E}_{\mathrm{slu}}$ without the presence of solvent charges and the average solute−solvent interaction energy $\langle \boldsymbol{U}_{\mathrm{slu-slv}} \rangle$, then the solute energy in solution is given by $\boldsymbol{E}_{\mathrm{slu}} = \boldsymbol{E}_{\mathrm{slu}}^{(\mathrm{total})} - \langle \boldsymbol{U}_{\mathrm{slu-slv}} \rangle$. We show $\boldsymbol{E}_{\mathrm{slu}}$ in Figure 8c, which is the difference between parts a and b of Figure 8. From this plot, we find that the solute energies of t-NMA and c-NMA are getting higher during the iteration and $\boldsymbol{E}_{\mathrm{slu}}$ of c-NMA is 6 kcal/mol, higher than that of t-NMA.

Table 1 is a summary of the dipole moments and solvation enthalpy of t-NMA and c-NMA. The calculated dipole moment of t-NMA in a vacuum is higher than experimental value. This problem has been discussed in refs 11 and 23. In our ab initio

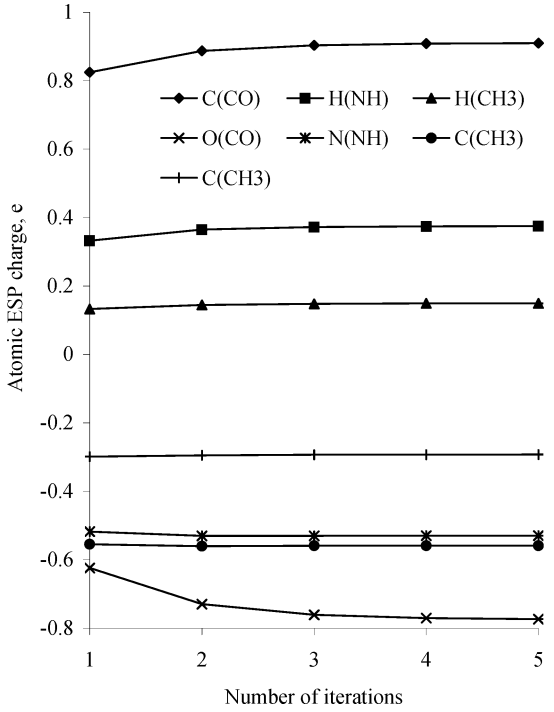

Figure 5. The atomic MEP-equivalent charges (ESP) of t-NMA as functions of QM/3d-RISM-HNC iterations. Calculations are at the RHF/6-31G(d) level in liquid water. 642 points are used for MEP fitting on the molecular surface.

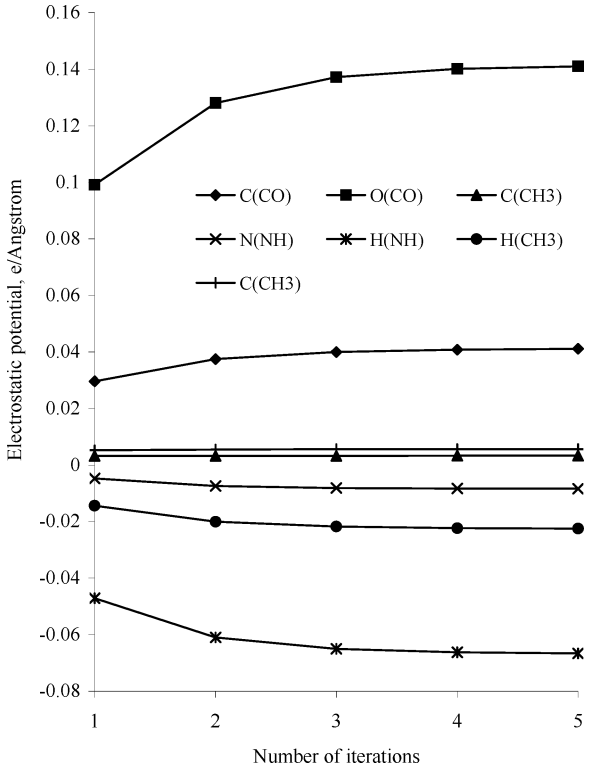

Figure 6. The solvent electrostatic potentials due to the solvent charge density on atoms of t-NMA as functions of QM/3d-RISM-HNC iterations.

calculations, the 6-31G(d) basis set is used. It is known that a good quality basis set with a polarization function is essential to achieve a good dipole moment.[23] Here we are mainly concerned with the relative value, i.e., polarization effect of the solvent. In our future studies, we would like to combine DFT with 3d-RISM-HNC and use quality basis sets to guarantee credible results for the dipole moment. In Table 1, the solvation

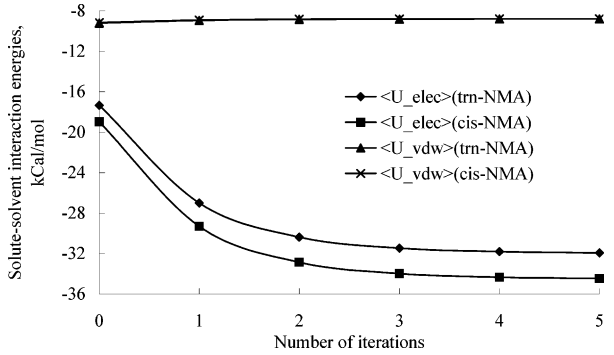

Figure 7. The average solute−solvent interaction energies of t-NMA and c-NMA in liquid water as functions of QM/3d-RISM-HNC iterations. The electrostatic part is getting stronger with iterations while the van der Waals part is quite flat.

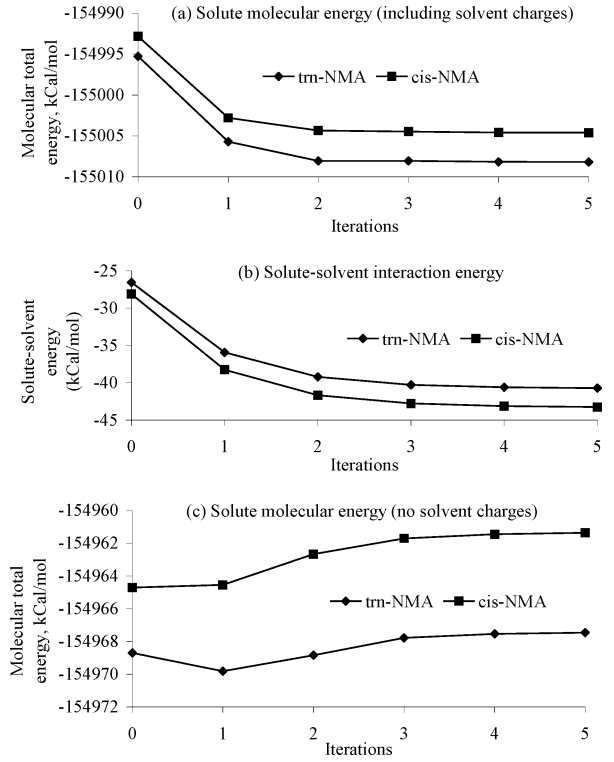

Figure 8. (a) The solute total energies of t-NMA and c-NMA as functions of QM/3d-RISM-HNC iterations. (b) The solute−solvent interaction energies (including electrostatic and van der Waals parts). (c) The solute total energies (not including solvent contributions), which are the differences between (a) and (b).

TABLE 1: The Dipole Moments (Debye) and Solvation Enthalpies (kcal/mol) of t-NMA and c-NMA

molecule	μ(gas)[a]	μ(gas)[b]	μ(aq)[c]	ΔE(aq−gas)[d] RHF−SCF	ΔE(aq−gas)[e] SCRF	Δh^f expt
t-NMA	3.51	4.22	5.79	−12.92	−8.82	−19
c-NMA		4.37	5.93	−11.80	−7.46	

[a] Experimental value, from ref 11. [b] RHF/6-31G(d), in a vacuum. [c] QM/3d-RISM-HNC, after five iteration cycles. [d] QM/3d-RISM-HNC, after five iteration cycles. [e] SCRF, 6-31G(d), a_0 = 6.18 Å, ϵ = 78. [f] Experimental value, from ref 24.

enthalpy of t-NMA calculated with SCRF, $\Delta \boldsymbol{E}^{(\mathrm{SCRF})} = \boldsymbol{E}_{\mathrm{aqu}}^{(\mathrm{SCRF})} - \boldsymbol{E}_{\mathrm{gas}}^{(\mathrm{SCRF})} = -8.82$ kcal/mol, is much smaller than the experimental value, −19 kcal/mol.[24,25] The dielectric constant used was $\epsilon = 78.0$, and a radius of spherical cavity $a_0 = 6.18$ Å is used in the SCRF calculations. The radius of the spherical cavity is a result of the RHF/6-31+G* calculations. The basis set 6-31+G* usually has been used in the calculations of

TABLE 2: The Average Solute−Solvent Electrostatic Interaction Energies $\langle U^{(elec)} \rangle$ of t-NMA and c-NMA (kcal/mol)

molecule	cycle 1[a]	cycle 1[b]	cycle 1[c]	cycle 5[a]	cycle 5[b]	cycle 5[c]
t-NMA	−17.34	−21.29	−22.53	−31.92	−32.66	−32.03
c-NMA	−18.96	−23.13	−24.47	−34.46	−35.12	−34.61

[a] Equations 14 and 15, classical Coulomb law, 128^3 grid. [b] Equations 10 and 12, quantum mechanics, 32^3 grid. [c] Equations 10 and 12, quantum mechanics, 128^3 grid.

molecular volume and radius of cavity in the SCRF method.[26−28] In our combined QM/3d-RISM-HNC, the solvation enthalpy is obtained in the RHF/6-31G(d) level. It is the difference between solute molecular energy in solution (after five iteration cycles) and that in the gas phase, $\Delta \boldsymbol{H}^{(RHF)} = \boldsymbol{E}_{aqu}^{(RHF)} - \boldsymbol{E}_{gas}^{(RHF)} = -12.92$ kcal/mol. This result is closer to the experimental value than that of SCRF.

In Table 2, we compare the solute−solvent average electrostatic interaction energies of t-NMA and c-NMA evaluated by quantum mechanical, eqs 10 and 12, and by classical Coulombic law, eqs 14 and 15, in a 32^3 cubic grid and in a 128^3 cubic grid, respectively. In the QM/3d-RISM-HNC iteration cycle 1, the result of classical eq 14 and the result of quantum eq 12 are quite different, >5 kcal/mol. However, after 5 iteration cycles of the combined QM/3d-RISM-HNC calculations, the difference is much smaller, <0.2 kcal/mol. Table 2 also shows that reduction of the solvent charges from a 128^3 grid to a 32^3 grid does not alter the energy significantly when computation converges, i.e., <0.5 kcal/mol.

V. Summary and Conclusion

The combined quantum mechanical and integral equation theory approach, QM/3d-RSIM-HNC, is able to give good description of the solute−solvent electrostatic interaction and polarization. In the QM/3d-RISM-HNC iteration procedure, the electronic structural change of the solute molecule in solution is given by quantum mechanics in solvent background charges obtained from the integral equation theory, and the structural change of the solvent molecule is described by 3d-RISM-HNC using ESP equivalent atomic charges obtained from the QM calculations. With examples used in this paper, i.e., t-NMA and c-NMA, the iterations converge smoothly after five to six cycles.

For the two systems we studied, i.e., t-NMA and c-NMA in liquid water, we see a significant increase of dipole moments, higher atomic solute charges, and an excess energy due to the presence of the solvent molecules. In the solvent part, we see higher water hydrogen density $\langle \rho_H(\mathbf{r}) \rangle$ on oxygen in the carbonyl group O (C═O) and higher water oxygen density $\langle \rho_O(\mathbf{r}) \rangle$ near H(NH) of t-NMA comparing with the pure 3d-RISM-HNC calculations. On these two positions, the hydrogen bonds are formed. The site−site interaction energies on these two atoms are very close to the experimental hydrogen bond energies after QM/3d-RISM-HNC iteration converged. This may serve as evidence that combined QM/3d-RISM-HNC calculations give credible electrostatic response and polarization of polar solute in polar solvents. One advantage of 3d-RISM-HNC is that the interaction sites could be assigned to any part of molecules, for example, atoms, atomic groups, or some parts in a molecule. This makes it valuable in the study of active sites of protein in aqueous solution, which often include charged side chains and polar groups.

The solvation enthalpy of t-NMA, −12.92 kcal/mol, as given by our calculation is closer to the experimental value, −19 kcal/mol,[24,25] and better than the result of SCRF, −8.82 kcal/mol. Further improvement is achieved after introducing hydrogen and oxygen bridge functions in our previous work,[15] which improve both the electrostatic part and the van der Waals part of the solute−solvent interaction energies effectively. Hopefully, in the future studies, after carefully selecting and optimizing parameters in 3d-RISM-HNC, we may achieve better quantitative results.

The dipole moment in the liquid phase is an important physical property, which describes the strength of the polarization effect. In the gas phase, the calculated dipole moment (4.22 D) of t-NMA at the RHF/6-31G(d) level is much bigger than the experimental value (3.51 D).[28] We have tried several basis sets and quantum mechanical methods, none of them give satisfied values. A larger basis set with polarization is the solution. Our future work will be focused on combining DFT with 3d-RISM-HNC, which may improve the speed of quantum calculations and have sufficient accuracy to study peptides and other biological systems.

Acknowledgment. Many thanks to Professor Benoit Roux, Department of Biochemistry, Medical College, Cornell University, for allowing us to use his 3d-RISM-HNC program. This work was supported by Research Grant (023618211) from Tinajin Municipal Science and Technology Commission, China.

References and Notes

(1) Barnes, P.; Quinn, J. E.; Finney, J. L.; Nicholas, J. D. *Nature* **1979**, *282*, 459.

(2) Van Belle, D.; Couplel, I.; Prevost, M.; Wodak, S. J. *J. Mol. Biol.* **1987**, *198*, 721.

(3) Dang, L. X.; Kollman, P. A.; Rice, J. E.; Caldwell, J. *J. Am. Chem. Soc.* **1991**, *113*, 2481.

(4) Sharp, K.; Honig, B.; Jean-Charles, A. *J. Phys. Chem.* **1992**, *96*, 3882.

(5) Warshel, A.; Levill, M. *J. Mol. Biol.* **1976**, *103*, 227.

(6) Chambers, C. C.; Hawkins, G. D.; Cramer, C. J.; Truhlar, D. G. *J. Phys. Chem.* **1996**, *100*, 16385.

(7) Stern, H. A.; Kaminski, G. A.; Banks, J. L.; Zhou, R.; Berne, B. J.; Friesner, R. A. *J. Phys. Chem. B* **1999**, *103*, 4730.

(8) Field, M. J.; Bash, P. A.; Karplus, M. *J. Comput. Chem.* **1990**, 700−733. Cui, Q.; Karplus, M. *J. Phys. Chem. B* **2002**, *106*, 1768.

(9) Wei, D. Q.; Salahub, D. R. *Chem. Phys. Lett.* **1994**, *224*, 291; *J. Chem. Phys.* **1994**, *101*, 7633.

(10) Weiner, S. T.; Kollman, P. A.; Case, D. A.; Singh, U. C.; Ghio, C.; Alagona, G.; Profeta, S.; Weiner, P. *J. Am. Chem. Soc.* **1984**, *106*, 765.

(11) Gao, J.; Xia, X. *Science* **1992**, *258*, 631. Gao, J. *J. Phys. Chem.* **1992**, *96*, 537. Vasilyev, V. V. *THEOCHEM* **1994**, *304*, 129. Thomson, M. A. *J. Am. Chem. Soc.* **1995**, *117*, 11341.

(12) Cramer, C. J.; Truhlar, D. G. In *Reviews in Computational Chemistry*; Lipkowitz, K. B., Ed.; VCH: New York, 1995.

(13) Chen, J. L.; Noodleman, L.; Case, D.; Bashford, D. A. *J. Phys. Chem.* **1994**, *98*, 11059. Miertus, S.; Scrocco, E.; Tomasi, J. *Chem. Phys.* **1981**, *55*, 117. Luque, F. J.; Illas, F.; Orozco, M. *J. Comput. Chem.* **1990**, *11*, 416. Luque, F. J.; Orozco, M. *Chem. Phys. Lett.* **1990**, *168*, 269.

(14) Ten-no, S.; Hirata, F.; Kato, S. *Chem. Phys. Lett.* **1993**, *224*, 391; *J. Chem. Phys.* **1994**, *100*, 7443. Sato, H.; Hirata, F.; Kato, S. *J. Chem. Phys.* **1996**, *105*, 1546. Sato, H.; Kovalenko, A.; Hirata, F. *J. Chem. Phys.* **2000**, *112*, 9463. Yoshida, N.; Kato, S. *J. Chem. Phys.* **2000**, *113*, 4974.

(15) Du, Q.; Beglov, D.; Roux, B. *J. Phys. Chem. B* **2000**, *104*, 796.

(16) Frisch, M. J.; Trucks, G. W.; Schlegel, H. B.; Gill, P. M. W.; Johnson, B. G.; Robb, M. A.; Cheeseman, J. R.; Keith, T.; Petersson, G. A.; Montgomery, J. A.; Raghavachari, K.; Al-Laham, M. A.; Zakrzewski, V. G.; Ortiz, J. V.; Foresman, J. B.; Cioslowski, J.; Stefanov, B. B.; Nanayakkara, A.; Challacombe, M.; Peng, C. Y.; Ayala, P. Y.; Chen, W.; Wong, M. W.; Andres, J. L.; Replogle, E. S.; Gomperts, R.; Martin, R. L.; Fox, D. J.; Binkley, J. S.; Defrees, D. J.; Baker, J.; Stewart, J. P.; Head-Gordon, M.; Gonzalez, C.; Pople, J. A. *Gaussian 94*, revision E.2; Gaussian, Inc.: Pittsburgh, PA, 1995.

(17) Roux, B. Yu, H.-A.; Karplus, M. *J. Phys. Chem.* **1994**, *94*, 4683−4688.

(18) Beglov, D.; Roux, B. *J. Chem. Phys.* **1994**, *100*, 9050; *J. Chem. Phys.* **1995**, **103**, 360; *J. Chem. Phys.* **1996**, *104*, 8678; *J. Phys. Chem.* **1997**, *101*, 7821.

(19) Jorgensen, W. L.; Chandrasekhar, J.; Madura, J. D.; Impey, R. W.; Klein, M. L. *J. Chem. Phys.* **1983**, *79*, 926.

(20) Hirata, F.; Rossky, P. J. *Chem. Phys. Lett.* **1981**, *83*, 329.
(21) Hall, G. G.; Smith, C. M. *Int. J. Quantum Chem.* **1984**, *25*, 881. Smith, C. M.; Hall, G. G. *Theor. Chim. Acta* **1986**, *69*, 63.
(22) Kovalendo, A.; Hirata, F. *J. Chem. Phys.* **2000**, *113*, 2793.
(23) Casida, M. E. In *Time-Dependent Density Functional Response Theory of Molecular Systems: Theory, Computational Methods, and Functionals*; Seminario, J. M., Ed.; Elsevier: Amsterdam, 1996; p 391.
(24) Wolfenden, R. *Biochemistry* **1978**, *17*, 201.
(25) Spencer, J. N.; Berger, S. C.; Powell, C. R.; Henning, B. D.; Furman, G. S.; Loffredo, W. M.; Rydgerg, E. M.; Neubert, R. A.; Shoop, C. E.; Blauch, D. N. *J. Phys. Chem.* **1981**, *85*, 1236.
(26) Wiberg, K. B.; Keith, T. A.; Frisch, M. J.; Murcko, M. *J. Phys. Chem.* **1995**, *99*, 9072. Wong, M. W.; Frisch, M. J.; Wiberg, K. B. *J. Am. Chem. Soc.* **1991**, *113*, 4776. Wong, M. W.; Wiberg, K. B.; Frisch, M. J. *J. Phys. Chem.* **1991**, **95**, 8991. Wong, M. W.; Wiberg, K. B.; Frisch, M. J. *J. Am. Chem. Soc.* **1992**, *114*, 1645. Wong, M. W.; Wiberg, K. B.; Frisch, M. J. *J. Am. Chem. Soc.* **1992**, *114*, 523.
(27) Karelson, M. M.; Tamm, T.; Katrizky, A. R.; Szefran, M.; Zerner, M. C. *Int. J. Quantum Chem.* **1990**, *37*, 1. Karelson, M. M.; Katrizky, A. R.; Zerner, M. C. *Int. J. Quantum Chem.* **1986**, *20*, 521.
(28) Gao, J. In *Modeling the hydrogen bond*; Smith, D. A., Ed.; ACS: Washington, DC, 1994.